Published online 23 December 2007

Nucleic Acids Research, 2008, Vol. 36, No. 4 ***1163–1175***
doi:10.1093/nar/gkm1130

Characterization of a ribonuclease III-like protein required for cleavage of the pre-rRNA in the 3′ETS in *Arabidopsis*

P. Comella, F. Pontvianne, S. Lahmy, F. Vignols, N. Barbezier, A. DeBures, E. Jobet, E. Brugidou, M. Echeverria and J. Sáez-Vásquez*

Laboratoire Génome et Développement des Plantes, UMR 5096 CNRS-UPVD-IRD, Université de Perpignan, 66860 Perpignan cedex, France

Received September 6, 2007; Revised December 4, 2007; Accepted December 5, 2007

ABSTRACT

Ribonuclease III (RNaseIII) is responsible for processing and maturation of RNA precursors into functional rRNA, mRNA and other small RNA. In contrast to bacterial and yeast cells, higher eukaryotes contain at least three classes of RNaseIII, including class IV or dicer-like proteins. Here, we describe the functional characterization of AtRTL2, an *Arabidopsis thaliana* RNaseIII-like protein that belongs to a small family of genes distinct from the dicer family. We demonstrate that AtRTL2 is required for 3′external transcribed spacer (ETS) cleavage of the pre-rRNA *in vivo*. AtRTL2 localizes in the nucleus and cytoplasm, a nuclear export signal (NES) in the N-terminal sequence probably controlling AtRTL2 cellular localization. The modeled 3D structure of the RNaseIII domain of AtRTL2 is similar to the bacterial RNaseIII domain, suggesting a comparable catalytic mechanism. However, unlike bacterial RNaseIII, the AtRTL2 protein forms a highly salt-resistant homodimer that is only disrupted on treatment with DTT. These data indicate that AtRTL2 may use a dimeric mechanism to cleave double-stranded RNA, but unlike bacterial or yeast RNase III proteins, AtRTL2 forms homodimers through formation of disulfide bonds, suggesting that redox conditions may operate to regulate the activity of RNaseIII.

INTRODUCTION

RNaseIII is a double-stranded RNA (ds-RNA) endonuclease found in bacteria and eukaryotic cells. It is involved in the processing of a large number of RNA substrates, including precursors of rRNA (1–3), snoRNA (4–8), snRNA (9,10), mRNA decay (11,12) and RNA interference (13). All members of the RNaseIII family contain a characteristic ribonuclease domain, which has a highly conserved stretch of nine amino acid residues known as the RNaseIII signature motif. RNaseIII proteins vary widely in length, from 200 to 2000 amino acids (14,15) and have been subdivided into four classes based on domain composition. Class I is the simplest and the smallest, containing a single ribonuclease domain and a dsRNA-binding domain (dsRBD); the bacterial and bacteriophage RNaseIII (15) belong to this class. Class II is identified by the presence of a highly variable N-terminal domain extension and includes the *S. cerevisiae* Rnt1 (16) and *S. pombe* Pac1 (17) proteins. Both of these yeast proteins are longer than bacterial RNaseIII and contain an additional ~100 amino acid fragment at the N-terminus. Class III, including Drosha proteins (14), has a dsRBD and two ribonuclease domains. Class IV, also referred to as Dicer, is the largest and contains two ribonuclease domains, a dsRBD, an N-terminal helicase and a PAZ domain (13–15).

In eukaryotic cells, class II and III enzymes are expected in the nucleus and participate in processing of snoRNA and rRNA precursors (14). In addition, it has been shown that nuclear and nucleolar localization of Rnt1 (18) and human RNaseIII (3) are cell-cycle regulated. Although RNaseIII class II has also been implicated in snRNA (9,10) and mRNA (11) cleavages, it is not clear where these processes take place. Class IV enzymes are found in the nucleus (19,20) and endoplasmic reticulum (21) and induce gene silencing.

Crystallization of an *Aquifex aeolicus* RNaseIII ribonuclease dimer provided the first insights into RNaseIII

*To whom correspondence should be addressed. Tel: +33 4 68 66 21 32; Fax: +33 4 68 66 84 99; Email: saez@univ-perp.fr
Present addresses:
Vignols F. and Brugidou C., IRD, Montpellier, France
Barbezier N., IGH/CNRS UPR 1142, Montpellier, France

The authors wish it to be known that, in their opinion, the first four authors should be regarded as joint First Authors.

active site organization and substrate recognition (22,23). These studies, together with biochemical evidence, led to a model where two ribonuclease domains combine to form a single processing center, each domain contributing to the hydrolysis of one RNA strand. In contrast to class III and class IV RNase, which are active as monomers and process dsRNA into small RNA fragments of ~21–27 nt, RNaseIII from class I or II are active as homodimers of two identical subunits, with dimerization occurring through the ribonuclease domain by hydrophobic interactions (23,24). This protein dimer degrades dsRNA to small duplex products of ~10–18 nt (13). It is also noteworthy that, unlike bacterial RNaseIII that forms only dimers (24), yeast Rnt1 protein forms additional high molecular weight complexes, suggesting that Rnt1 possesses two mechanisms of dimerization (25). In fact, the N-terminus of Rnt1p contains a dimerization signal involved in the multimerization of Rnt1 and is also required for efficient RNA cleavage (25). However, these results remain controversial since similar experiments carried out by Nagel and Ares show that the N-terminal domain of Rnt1p is not required for dimerization or RNA cleavage (26).

In *E. coli*, typical RNaseIII substrates are cellular or viral RNA that are able to form double-stranded RNA. Although recognition elements that direct RNaseIII-mediated cleavage have been identified, no clear consensus sequence has been defined [(27) and references therein]. In yeast Rnt1, the dsRBD recognizes its substrate by interacting with stems of capped RNA with conserved AGNN (28) or AAGU (29) tetraloops. Recognition of the tetraloop by the dsRBD locates the ribonuclease domain on the cleavage site, which is 13–16 bp from the tetraloop, in a ruler like mechanism (28). Interestingly, it has recently been shown that Rnt1 can bind short RNAs and use them to direct sequence-specific RNA degradation (30).

Higher eukaryotic organisms possess either one RNaseIII isoform from class II or III and at least one RNaseIII isoform from class IV. However, most of our knowledge of class II RNaseIII comes from yeast Rnt1 studies [(6,11,18,25,29,31) and references therein] and little is known about this class of RNaseIII in other eukaryotic organisms.

In plants, the genome of *Arabidopsis thaliana* encodes four RNaseIII proteins gene from class IV (32,33) and three other uncharacterized RNaseIII-like protein genes [(19) and this study]. The function and molecular basis of the four RNaseIII–dicer proteins in small RNA metabolism, gene silencing and DNA methylation have been extensively studied (34–40). However, the identification and molecular characterization of the other RNaseIII proteins involved in ribosome biogenesis and the metabolism of other RNA substrates remain unknown.

Here, we characterized the *A. thaliana* RTL2 protein, a class II RNaseIII-like protein that cleaves pre-rRNA precursors in the 3′ETS. AtRTL2 protein expression is regulated during plant development and the nuclear–cytoplasm localization is controlled by a novel nuclear export signal. AtRTL2 cleaves double-stranded RNA by a catalytic mechanism similar to bacteria and yeast; however unlike bacterial RNaseIII and yeast Rnt1 proteins, AtRTL2 dimerizes through the formation of disulfide bonds. In summary, this is the first demonstration of the involvement of RNaseIII in the cleavage of the 3′ETS of pre-rRNA in a higher eukaryotic organism. It also reveals that redox mechanisms are involved in the control of RNaseIII in plants.

MATERIALS AND METHODS

Identification and cloning of RTL1, RTL2 and RTL3 genes

Cloning of full-length cDNA sequence encoding RTL1 was performed by reverse transcription polymerase chain reaction (RT-PCR) with total RNA isolated from *A. thaliana* roots (see below). Primers used for amplification were designed from a truncated cDNA clone (BE529433) and the genomic sequence FCAALL using the Genscan program (http://genes.mit.edu/GENSCAN.html). The cloned cDNA is different from the annotated *RTL1* gene (At4g15417, data not shown). It has 25 more amino acids at the N-terminus and contains an additional exon of 51 amino acids in the C-terminal sequence. The *RTL1* gene reported here is different from that reported previously (19). The former encodes a protein containing an RNA binding but not an RNaseIII domain (19) and consequently we decided to retain the name *AtRTL1*. The *AtRTL2* (At3g20420) cDNA clone sequence BE522666 was obtained from the ABRC DNA Stock Center. The *RTL3* gene corresponds to the At5g45150 annotated gene sequence. All clones used in this study were sequenced with a model 3100 DNA sequencer and an ABI PRISM Big Dye Terminator Cycle Sequencing Ready Reaction Kit (Applied Biosystems, Foster City, CA).

Bioinformatic analysis

RNaseIII and RNA-binding domains were identified using Motif Scan software (http://hits.isb-sib.ch/cgi-bin/PFSCAN). The phylogenetic tree of RNaseIII and dicer proteins was generated with MEGA3.1 software (41), using the Neighbor Joining method coupled with 1000 bootstrap tests. The amino acid sequence of Dicer, Dicer-like proteins, RNaseIII and RNaseIII-like proteins were obtained from the National Center for Biotechnology Information (http://www.ncbi.nlm.nih.gov) and the Arabidopsis Information Resource (http://www.arabidopsis.org). The RTL2 protein model was generated with SWISS-MODEL, based on the *A. aeolicus* RNaseIII protein structure model (23), and visualized with RASMOL 2.7.2.1.1 software (57). GeneVestigator (www.genevestigator.ethz.ch) and Arabidopsis eFP (http://bbc.botany.utoronto.ca) browsers were used to compare RT-PCR results obtained in this study with digital northerns.

Plant growth conditions and mutant isolation

All lines were derived from *A. thaliana* Columbia (Col 0 ecotype) and cultivated as described previously (42). Seeds corresponding to *AtRtl2* plant lines were obtained

from the GABI-Kat/ADIS Stock Center (http://mpiz-koeln.mpg.de).

Methods related to RNA

Total RNA from plant organs and tissues was extracted from 15-day-old *A. thaliana* plantlets using TriZol reagent (GE Healthcare, Littler Chalfont, Bukimhamshire, UK). After treatment with RQ1 RNase-free DNase (Promega, Madison, WI) to eliminate contaminant DNA, first strand cDNA synthesis was performed on 5 µg of total RNA using the ProSTAR First-strand RT-PCR kit following the manufacturer's instructions (Stratagene, La Jolla, CA). To ensure that the amount of the amplified products remains in linear proportion, a semi-quantitative PCR reaction of 25 cycles (EF1α) or 31 cycles (*RTL1*, *RTL2* and *RTL3*) was performed using a PTC-200 (MJ Research, Watertown, MA). PCR products were cloned into pGEM-T Easy vector (Promega) and sequenced with T7 and SP6 primers.

Expression of His-RTL2 and production of antibodies

A cDNA fragment encoding amino acids from 1 to 391 of RTL2 was amplified by PCR from an EST clone (accession no. BE522666) using primers *5′rtl2*-XhoI and *3′rtl2*-BamHI. This fragment was cloned into the XhoI/BamHI site of the plasmid pET16b (Novagen, Madison, WI) to produce the His-tagged-RTL2 recombinant fusion protein. The recombinant fusion protein His-AtRTL2 was produced following Novagen's instructions. After cell disruption, the expressed fusion protein was recovered by centrifugation in the insoluble fraction. For protein purification, inclusion bodies were suspended in 10 ml of cold 20 mM Tris–HCl pH 7.5, 6 M urea and the His-AtRTL2 recombinant protein purified using a Ni^{2+} column HiTrap Chelating HP following Pharmacia's instructions (GE Healthcare). For protein refolding, purified His-AtRTL2 recombinant protein was successively dialyzed for 2 h against 20 mM Tris-HCl, pH 7.5; 500 mM NaCl buffer containing 6, 4, 2, 1, 0.5 or 0.1 M urea. A final dialysis step was performed overnight against 0 M urea buffer. Then, one volume of 86% glycerol was added to the dialyzed fraction and stored at −20°C for further characterization. For antibody production, a rabbit polyclonal antibody against His-AtRTL2 fusion protein was customer-made by Eurogentec (Seraing, Belgium). The IgG fractions from the antisera were purified through a HiTrap Protein A affinity column from Amersham Pharmacia Biotech (GE Healthcare).

Methods related to proteins

Plant material (0.2 g) was homogenized and extracted in 2 ml of 50 mM Tris–HCl pH 8, 150 mM NaCl, 10 mM EDTA, 50 mM NaF, 1% NP40, 0.5% sodium desoxycholate, 0.1% SDS, 1 mM PMSF, 10 mM β-mercaptoethanol (βME) and 20 µl of anti-protease cocktail (Sigma). The extracts were cleared by centrifugation at 13 000*g* for 15 min and conserved at −80°C. To obtain nuclear protein extracts, 2 g of 14-day-old seedlings were ground in a mortar and homogenized in 10 ml of nuclear extraction buffer (0.5 M Hexylene Glycol, 0.01 M $MgCl_2$, 0.05 M MOPS, pH 7.0). All subsequent steps were carried out in a cold room at 4°C. The homogenate was filtered through 60 µm nylon and Triton X-100 was added to a final concentration of 1%. After 10 min incubation, the homogenate was layered onto a 35% (4 ml) and 80% (3 ml) Percoll (SIGMA-Aldrich, St Louis, MO) step gradient in extraction buffer. After centrifugation for 30 min at 1090*g*, the nuclear fraction, located at the interface, was collected and washed twice with nuclear extraction buffer and stored at −80°C. Nuclear proteins were extracted in SDS-sample buffer (43) and analyzed by 10% SDS–PAGE. Western blots were performed as previously described (44). The membranes were hybridized with a 1:4000 dilution of α-AtRTL2 or a 1:5000 dilution of α-AtNUC1 (42) or α-NTR (45).

Gel filtration chromatography

Flower bud extracts were prepared in protein extraction buffer (PEB, 20 mM HCl–Tris pH 7.9, 0.2 mM EDTA, 20% Glycerol) containing either 100 mM KCl (PEB100) or 500 mM KCl (PEB500), centrifuged for 20 min at 48 400*g* and the supernatant filtered through a 0.45 µm filter (Gelman Sciences). Approximately 400 µg of soluble proteins were loaded directly onto a Hi-Prep 16/60 Sephacryl S300 HR (GE Healthcare) column equilibrated and run either in PEB100 or PEB500. For western blot analysis, 200 µl of 1 ml fractions were precipitated with 4 volumes of cold acetone and the pellet dissolved in SDS loading buffer (43). The protein standards for size estimation of RTL2 were alcohol dehydrogenase, 150 kDa and BSA, 66 kDa (SIGMA).

Cellular localization studies of RTL2 in onion cells

The *AtRTL2* cDNA sequence was amplified by PCR using primers *5′rtl2-NcoI* and *3′rtl2-NcoI*. This fragment was cloned into the NcoI site of the plasmid ppK100 (46) to produce the RTL2::GFP recombinant fusion protein. To fuse the N-terminal sequence of AtRTL2 to the GUS:NLS plasmid (47), the DNA sequence encoding amino acids 1 to 59 was amplified by PCR using primers *5′rtl2-NcoI* and *3′del59rtl2-NcoI*. This fragment was cloned into the NcoI site located in the N-terminal sequence of GUS. For transient expression, 5 µg of plasmid was coated to 1.6 µm gold particles (BioRad, Hercules, CA) according to the BioRad transformation protocol. Onion epidermal layers were transfected using the PDS-1000/He biolistic. All GUS and GFP microscopic images were taken using a Zeiss Axioskop 2 microscope and recorded using a Leica DC 300 FX digital camera (Leica).

Treatment of proteins with redox agent DTT

For redox treatment, recombinant protein was diluted tenfold with 50 mM Tris–HCl pH 8.0, 150 mM NaCl, 10 mM EDTA, 1% NP40 buffer. Protein samples were incubated with a 1/4 volume of SDS-sample buffer (43) containing either 500; 50, 5 or 0.5 mM DTT. After boiling for 1 min, samples were loaded onto an SDS–PAGE as described before.

Primers used in this work

5′rtl1: CATGAACAAGACACAAACACAACAG
3′rtl1: CCTCATGACAAGGTCTCCGAAAAATTTAG CAAAATTGTC
5′rtl2: ATGGATCACTCTATCTCACCGGAG
3′rtl2: GGCTCTAATCATGTGATACGCCG
5′rtl3: ATGGATTCT TCAGTGGAAGCA
5′rtl3: ATGAATTCAGTAGAAGCAGTA
3′rtl3: TAGTCTTCTCCTCCTCTTTG
5′rtl2-XhoI: CCGCTCGAGGATCACTCTATCTCACCGGAGTAC
3′rtl2-BamHI: CGGGATCCTTAGAGATAATGAGAT TTTCTCAAGGC
rt-rtl2: CGCTTCCTTGAGAAGACTCTTGTTAC
5′eIF1α: ctaaggatggtcagacccg
3′eIF1α: cttcaggtatgaagacacc
5′3ETS: CCCAACTTTACACGAGCTCG
3′3ETS: CCTCGGACCCGGTAAAC
5′U3: ACGGACCTTACTTGAACAGGATCTG
3′U3: CTGTCAGACCGCCGTGCGA
5′R82: CGTTTCTGTGTCGATAACCCCGCTG
3′R84: CAAGTGTTGGATTAGATTAATTTTGC
5′tRNA: caacaaagcaccagtggtc
3′snoRNA: GAGAATGCATTGGACCCAACCAATAC
5′rtl2-NcoI: CATGCCATGGCAGATCACTCTATCTC ACCGGAGTAC
3′rtl2-NcoI: CATGCCATGGCGAGATAATGAGATTT TCTCAAGGC
3′del59rtl2-NcoI: AAGCCATGGCCTCCGACGAAACCGGAACGC

RESULTS

The *A. thaliana* genome contains three RNase III-like genes

In order to identify RNaseIII-like proteins in *A. thaliana*, we performed a Blast search using RNaseIII protein from *E. coli* and Rnt1 from yeast. Seven genes coding for proteins containing the RNaseIII motif were found in the *Arabidopsis* genome. Four belong to the DCL family (32,33) and the three others to a new uncharacterized family of RNaseIII genes in *Arabidopsis* (Figure 1). We initiated the molecular and functional characterization of this new family of genes, namely *AtRTL1, AtRTL2* and *AtRTL3 (RNAse Three Like1, 2* and *3)*. The deduced AtRTL1, AtRTL2 and AtRTL3 proteins are 289, 391 and 957 amino acids long with predicted molecular masses of 33, 45 and 108 kDa, respectively. All three sequences contain either one (AtRTL1 and AtRTL2) or two (AtRTL3) RNaseIII domains (Figure 1A). The highly conserved stretch of 9 amino acid residues known as the RNaseIII signature motif (14) is well conserved in AtRTL1 and AtRTL2 sequences but only in the second RNaseIII motif of AtRTL3 (Figure 2B and data not shown). Furthermore, whereas AtRTL2 and AtRTL3 display two and three RNA-binding domains (RBD) respectively, the single putative RBD domain of AtRTL1 seems much less conserved or inexistant (Figure 1A). No other particular protein domains were identified in these three AtRTL sequences. Thus, *Arabidopsis* RTL proteins

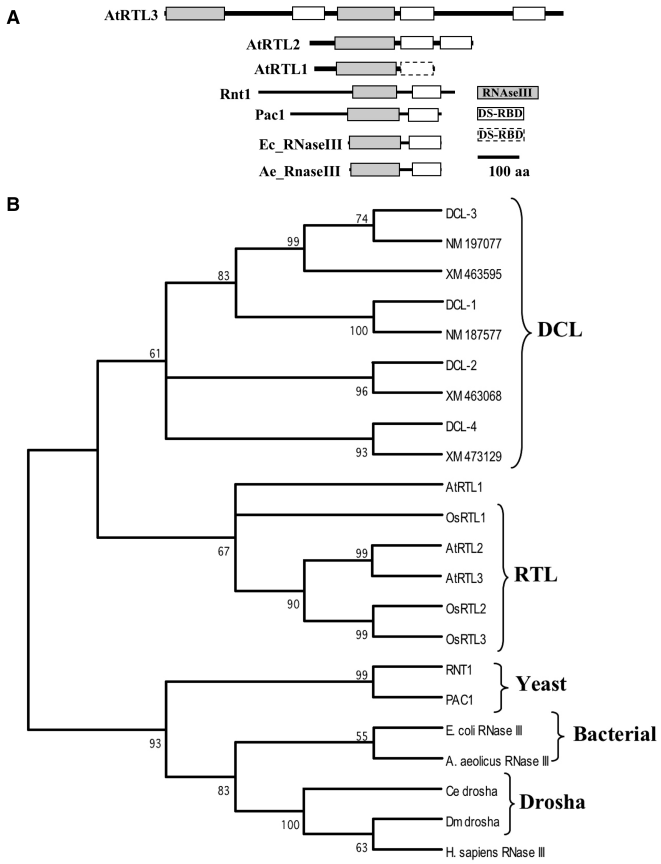

Figure 1. The *A. thaliana* genome encodes three RNase III-like proteins that belong to a distinct, non-dicer, gene family. (**A**) Schematic representation of RNaseIII and RNaseIII-like proteins from *A. thaliana* (AtRTL1, AtRTL2 and AtRTL3), *S. cerevisiae* (Rnt1), *S. pombe* (PacI), *E. coli* (Ec_RNaseIII) and *A. aeolicus* (Aa_RNaseIII). Gray boxes correspond to RNaseIII motifs, white boxes to double-strand RNA-binding domain (DS-RBD) and dotted white box in AtRTL1 to less conserved RBD. Black bars correspond to 100 amino acid length. (**B**) Phylogenetic relation of different RNaseIII and RNase-like proteins. Numbers represent the percentage value of Bootstrap. Accession numbers of sequences used in this analysis: *A. thaliana* DCL1 (At1g01040), DCL2 (At3g03300), DLC3 (At3g43920), DCL4 (At5g20320), AtRTL1 (this study), AtRTL2 (At3g20420) and AtRTL3 (At5g45150); *O. sativa* dicer-like proteins (available in the tree), OsRTL1 (Os06g0358800), OsRTL2 (Os05g0271300) and OsRTL3 (Os01g0551100), *S. cerevisiae* (AAB04172), *S. pombe* (NP_595292), *E. coli* (NP_417062), *A. aeolicus* (NP_213645); *C. elegans* (NP_501789.1), *D. melanogaster* (NP_477436.1) and *H. sapiens* (NP_037367.21).

do not belong to the *Arabidopsis* Dicer family which encodes larger proteins (from 1300 to 1900 amino acids long) containing multifunctional domains such as DExHRNA helicase, Piwi/Argonaute/Zwille (PAZ), RNase III and RBD (32,33). Similarly, *Arabidopsis* RTL protein structure is distinct from human RNaseIII and Drosha proteins that are 1374 and 1327 amino acids long respectively (3,14). Conversely, the *Arabidopsis* RTL1 and RTL2 proteins show structural similarity to bacterial RNaseIII (15,23), *S. cerevisiae* Rnt1 (48) and *S. pombe* Pac1 (17) proteins. However, the N-terminal sequences of RTL1 and RTL2 proteins are longer than bacterial RNaseIII but shorter than Rnt1 and Pac1 yeast RNaseIII-like proteins, which present an additional

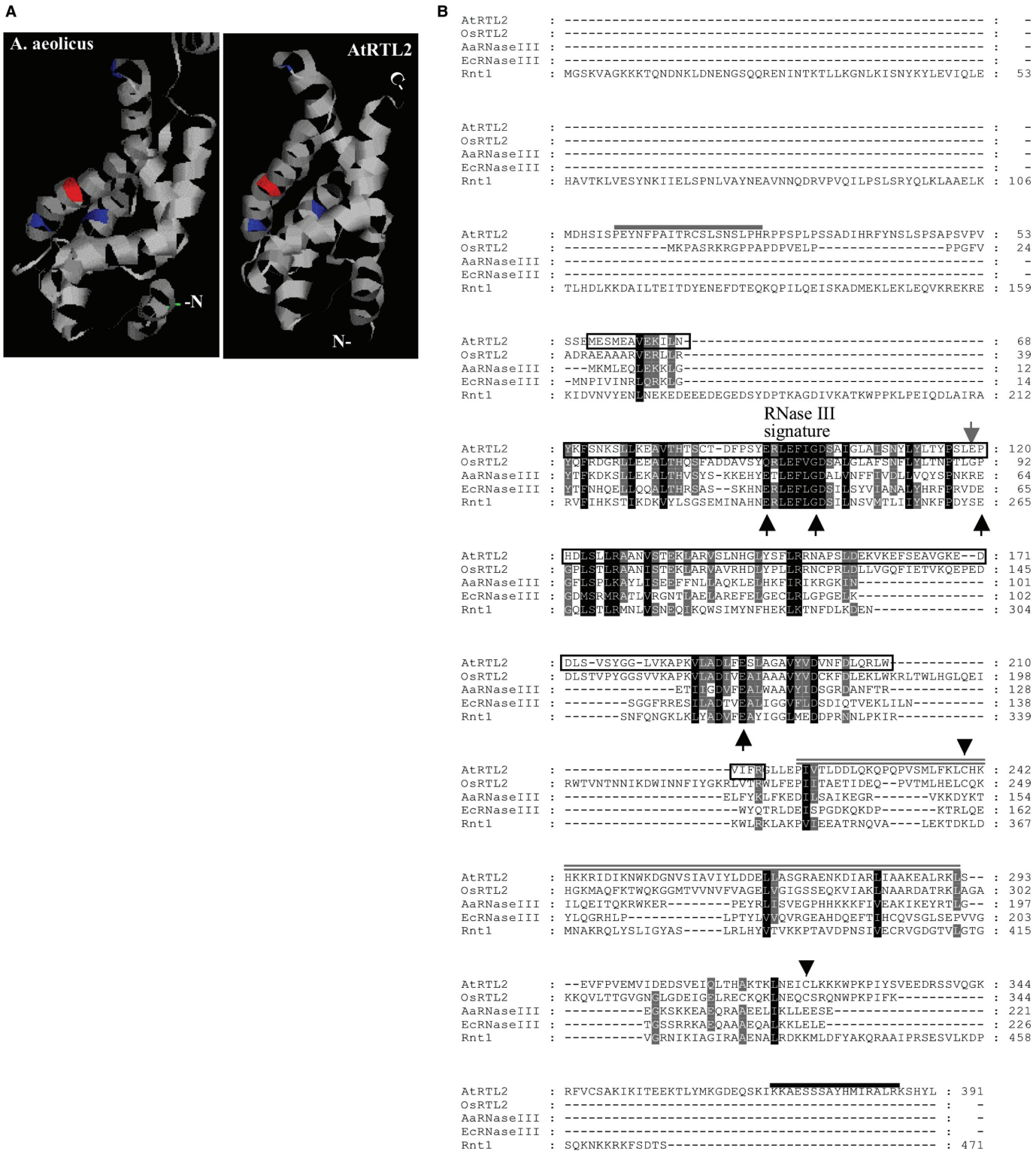

Figure 2. *In silico* analysis of the AtRTL2 sequence suggests a novel mechanism for RNaseIII activity in plants. (**A**) Comparison of the crystal structure of *A. aeolicus* RNaseIII protein domain (residues 1–147) and modeled AtRTL2 (residues 57–214). Blue boxes show residues E93, E119 and E165 (E37, E64 and E110 in *A. aeolicus*) and the red box shows residue D100 (D44 in *A. aeolicus*), located in the RNaseIII domain and proposed as RNA cutting sites. (**B**) Amino acid sequence alignment of AtRTL2, OsRTL2, bacterial RNaseIII (*E. coli* and *A. aeolicus*) and yeast Rnt1 proteins. Conserved amino acids are shaded black and gray. The 9 amino acid signature is indicated. The gray bar shows a potential nuclear export signal (NES), the double over lining shows predicted double-stranded RNA-binding domains (Ds-RBD) and the black bar the putative bi-partite nuclear localization signal (bi-NLS). The modeled AtRTL2 sequence (residues 57–214) is boxed. Black arrowheads show the two conserved cysteines in AtRTL2 and OsRTL2 and potentially required for protein dimerization. Black arrows show proposed RNA cutting site residues in the bacterial sequence. The gray arrow shows the glutamic acid residue shown in the predicted structure of RTL2.

100 amino acid sequence in their N-terminal region (Figures 1A and 2B).

Phylogenetic analysis using entire RNaseIII sequences showed that AtRTL1, -2 and -3 sequences from *A. thaliana* form a plant-specific RNaseIII group distinct from the *Arabidopsis* Dicer family in plants, yeast Rnt1 and Pac1 proteins, Drosha or bacterial and human RNaseIII (Figure 1B). This analysis also shows that *Arabidopsis RTL1*, *RTL2* and *RTL3* genes diverged from a common ancestor and that the *RTL2* and *RTL3* genes, as well as the orthologous genes in rice, result from recent independent duplication events in monocotyledons and dicotyledons.

The structural and sequence analysis of these AtRTL proteins suggests that the *AtRLT2* gene is the closest functional homolog of the RNaseIII and the Rnt1 protein genes. Moreover, we demonstrated that only AtRTL2 is ubiquitously expressed in *Arabidopsis* plants (see below). Thus, based on these observations, we selected the *AtRTL2* gene for further studies to unravel RNaseIII functions in higher eukaryotic cells.

Modeling of AtRTL2 protein reveals conserved RNaseIII catalytic domain but not RNA-binding domain structure

As mentioned before, RNaseIII is a double-stranded RNA (dsRNA) endonuclease and the active form is a homodimer of two identical RNaseIII polypeptides. In order to obtain insight into the role and mode of action of AtRTL2, we compared the predicted folded RTL2 *Arabidopsis* protein with the crystal structure of bacterial *A. aeolicus* RNaseIII (22,23). The AtRTL2 polypeptide chain fold adopted a similar structure to that of the RNaseIII domain of *Aa*-RNaseIII (Figure 2A). The analysis revealed a 28% sequence similarity between residues 57-214 of AtRTL2 and residues 1-147 of *Aa*-RNaseIII (Figure 2B). Moreover, both in *A. aeolicus* and *A. thaliana* sequences, conserved amino acids E37, D44, E64 and E110 (E93; D100, E119 and E165 in AtRTL2), which are part of the signature and proposed RNA cutting site residues (23), are located at the surface of two molecules that forms an active valley (shown in blue and red in Figure 2A). In contrast to the significant structural homology between the RNaseIII protein domains of *A. aeolicus* and *A. thaliana*, the C-terminal domain of AtRTL2 did not exhibit such structure homology. Indeed, we could not obtain a predicted folded structure based on the C-terminal domain of *A. aeolicus* or with crystallized dsRBD structures of RNaseIII and Rnt1 from *E. coli* (49) or *S. cerevisiae* (50), respectively.

The AtRTL2 gene is constitutively expressed in *A. thaliana*

To test expression of *AtRTL1*, *AtRTL2* and *AtRTL3* genes, we performed a semi-quantitative RT-PCR analysis. As shown in Figure 3, primers *5′rtl1* and *3′rtl1* amplify a band of ~0.6 kbp in roots only (lane 2, panel AtRTL1). Extended PCR times did not allow us to detect amplification in other tissues. On the other hand, primers *5′rtl2* and *3′rtl2* gave a weak band of ~1.2 kbp in roots, whereas greater amounts of the corresponding cDNA were

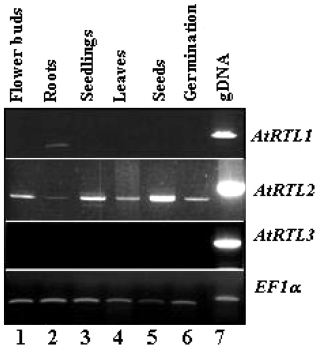

Figure 3. *AtRTL1*, *AtRTL2* and *AtRTL3* gene expression in *A. thaliana* plants. RT-PCR analysis of *AtRTL1, -2 and -3* in: flowers buds (lane 1), roots (lane 2), seedlings (lane 3), leaves (lane 4), seeds (lane 5) and germinating seeds (lane 6). *Arabidopsis thaliana* elongation factor 1α (*EF-1α*) gene expression was analyzed as a PCR control to evaluate the amount of cDNA used in each reaction (lanes 1–6). Lane 7, PCR amplification control using genomic DNA.

detected in flower buds, seedlings, leaves, dry seeds and 6-h germinating seeds (lanes 1–6, panel *AtRTL2*). We confirmed by sequencing that these bands correspond to specific *AtRTL1* and *AtRTL2* transcripts and not to genomic sequences, which produce ~0.7 and 1.3 kbp bands containing intron sequences (lane 7). Our data were consistent with electronic data from e-FP (51) and Genevestigator (www.genevestigator.ethz.ch) browsers. PCR amplification using primers *5′rtl3* and *3′rtl3* did not detect specific *AtRTL3* transcripts in these samples (lanes 1–6, panel *AtRTL3*), nor were transcripts detected using an internal primer located just upstream of the second RNaseIII motif of AtRTL3 (data not shown). PCR reactions using specific primers to amplify *EF1α* transcripts were used to verify amounts of cDNA in each reaction (lanes 1–6, panel *EF1α*).

Based on this study; it is likely that only *AtRTL1* and *AtRTL2* are functional genes in *Arabidopsis* plants grown in normal conditions. However, because *AtRTL2* is ubiquitously expressed, we suspected that the corresponding AtRTL2 protein could fulfil most RNase III activities of the cell.

AtRTL2 protein is expressed during seed maturation and germination

AtRTL2 transcripts are detected in all tissues and plant organs tested, including dry and germinating seeds (Figure 3). In order to study the protein expression of AtRTL2 during early stages of plant development, we produced polyclonal antibodies against a His-tagged recombinant AtRTL2 protein and performed western blot analysis of total soluble proteins extracted from flowers, siliques and seeds at different development stages and germinating seeds after a cold treatment period (4°C) of 48 h. As shown in Figure 4, the AtRTL2 protein level decreases over 13 days after fertilization (DAF) to become undetectable at 16 DAF (lanes 1–7). However, AtRTL2 protein became detectable again 6 h after seed imbibition (lanes 8–10) and its level remained stable after 24 and 48 h

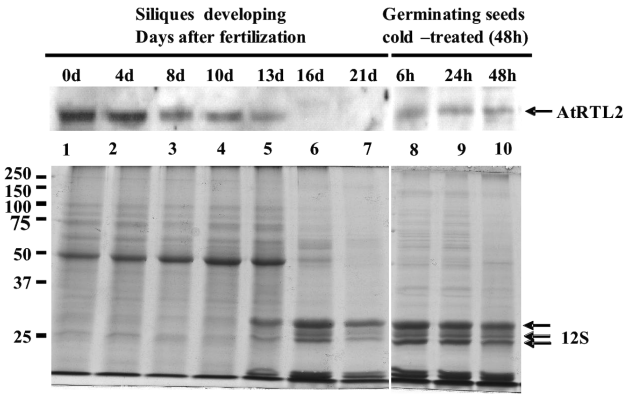

Figure 4. AtRTL2 protein is expressed during seed maturation and germination. Western blot analyses of AtRTL2 expression during seed development at 0, 4, 8, 10 13, 16 and 21 days after fertilization (lanes 1–7) and 6, 24 and 48 h after imbibition (lanes 8–10). Gel protein loading was verified by staining the gel with Coomassie blue. Seed development can be visualized by accumulation of 12S proteins (lanes 5–10).

germination (lanes 9–10). The SDS–PAGE stained with Coomassie blue is shown to control similar amounts of proteins of each sample and to visualize accumulation of 12 S storage proteins during seed development (52).

Nuclear cytoplasmic localization of AtRTL2 protein

To determine the *in vivo* sub-cellular localization of AtRTL2 we transformed epidermal onion cells by bombardment using an AtRTL2::GFP plasmid. As shown in Figure 5A, in transiently transformed onion cells the AtRTL2::GFP fusion protein was found in the nucleoplasm and the nucleus (top). The nucleus of onion cells is easily visualized by Nomarski and the GFP fluorescence co-localizes with this structure (middle). Transformation of onion cells with GFP plasmid alone, used as a control, shows homogenous fluorescence in the cell (bottom).

To confirm the nuclear and the cytoplasmic localization of AtRTL2, we performed western blot analysis using antibodies against the His-AtRTL2 recombinant protein. As shown in Figure 3B, antibodies against His-AtRTL2 (α-AtRTL2) cross-reacted with a single ~45 kDa polypeptide in the nuclear protein extract (Figure 5B, lane 2). The observed polypeptide corresponds to the ~45 kDa expected size of AtRTL2. When a total soluble protein extract was analyzed with the α-AtRTL2 antibody, a second band of ~43 kDa was detected (Figure 5B, lane 1). Analysis of *Atrtl2* plant mutants (see below) demonstrates that this band corresponds to a non-specific cross reaction. The nuclear protein extract was controlled with antibodies against the nuclear and nucleolar *A. thaliana* nucleolin-like 1 protein, AtNUC-L1 (42) (Figure 5B, α-AtNUC1 panel). As expected, AtNUC-L1 was mainly detected in the nuclear fraction (lane 4) when compared with total soluble proteins (lane 3), indicating that nuclear protein extract is enriched in nuclear proteins. In order to rule out contamination of the nuclear extract with cytoplasm, the same membrane was incubated with antibodies recognizing both NTRA and NTRB proteins, two NADPH Thioredoxin Reductases (NTR) (45) (Figure 5B, α-NTR panel). The α-NTR antibodies failed to detect any protein in the nuclear fraction (lane 4), whereas NTR proteins were easily detectable in the total soluble protein extract (lane 3).

In conclusion, these results clearly establish the cytoplasmic and nuclear localization of RTL2 in *A. thaliana*.

AtRTL2 contains N-terminal nuclear export signal

Nucleo-cytoplasmic partitioning of many transcription factors or enzymes is determined by the relative accessibility of nuclear export signals or NES (53). AtRTL2 contains a putative bipartite nuclear localization signal in the C-terminal sequence and a NES in the N-terminus (Figures 2B and 6). Comparison of NES from HIV-1Rev (54), mPKIa (55) and NES from Pap1 (56) highlights a similarity between the putative NES of AtRTL2 and *S. pombe* Pap1; in particular the residues CS located just before or after the third leucine in AtRTL2 and Pap1 sequences (Figure 6A, top). To determine if the putative NES of AtRTL2 was able to exhibit nuclear export activity, we fused the N-terminal sequence of AtRTL2 (amino acids 1–26) to a GUS::NLS fusion protein (47) to produce an NES::GUS::NLS fusion protein (Figure 6A, bottom). Transient expression experiments in onion cells show that the putative NES sequence of AtRTL2 is indeed able to export the GUS activity of the GUS–NLS fusion protein from the nucleus to the cytosol (Figure 6B), since the GUS labeling obtained with GUS::NLS alone (middle panel) decreases in the nucleus (bottom panel). Interestingly, NES from RTL2 is not able to translocate what seems to be some nucleolar localization of the GUS::NLS fusion construct (compare panels GUS::NLS panel versus NES::GUS::NLS panel). Transformation of onion cells with GUS plasmid alone, used as a control, shows homogenous GUS staining (GUS panel).

AtRTL2 forms dimer through disulfite bond formation

A significant difference can be noted between the plant AtRTL2 and yeast Rnt1 proteins. As observed in Figures 1A and 2B, the yeast Rnt1 protein shows an extended N-terminal sequence proposed to contain a dimerization signal (25). This domain is present neither in the *Arabidopsis* AtRTL2, nor in the rice ortholog OsRTL2. This raises the question as to whether plant RTL2 proteins are capable of dimerization like their yeast homologs, and how dimerization may occur. To attempt to answer the first question, we tried to obtain functional complementation of yeast Δ*rnt1* mutant cells by ectopic expression of AtRTL2. In *S. cerevisiae*, disruption of the *RNT1* gene is not lethal but leads to a strong growth defect (5). Despite the use of either low copy or high copy shuttle vectors, as well as strong promoters to produce AtRTL2 in yeast mutant cells, no complementation could be obtained (data not shown), indicating that AtRTL2 may function in a different manner to Rnt1 *in vivo*. In this context, to determine if AtRTL2 forms homodimers, total

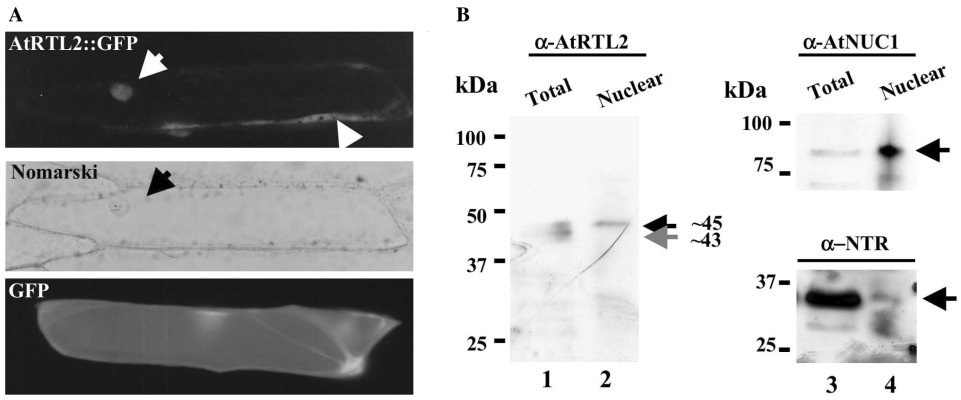

Figure 5. Nuclear and cytoplasmic localization of AtRTL2. (**A**) Cellular localization of AtRTL2::GFP fusion protein in transfected onion epidermis cells. Arrows point to the nucleus and cytoplasm visualized by GFP fluorescence (Upper panel); the nucleus can be easily observed by Nomarski (Middle panel). Onion epidermial cells transformed with GFP alone produce homogenous GFP fluorescence (Lower panel). (**B**) Immunolocalization of AtRTL2. Total soluble (lanes 1 and 3) and nuclear (lanes 2 and 4) protein extracts isolated from *A. thaliana* seedlings were separated by SDS–PAGE, transferred to nitrocellulose and incubated with α-AtRTL2 (left panel) or with α-AtNUC1 and α-NTR (right panel) antibodies. α-AtNUC1 antibody detects nuclear and nucleolar *Arabidopsis* nucleolin like-1 protein. α-NTR detects cytoplasmic *Arabidopsis* NADPH-thioredoxin reductase.

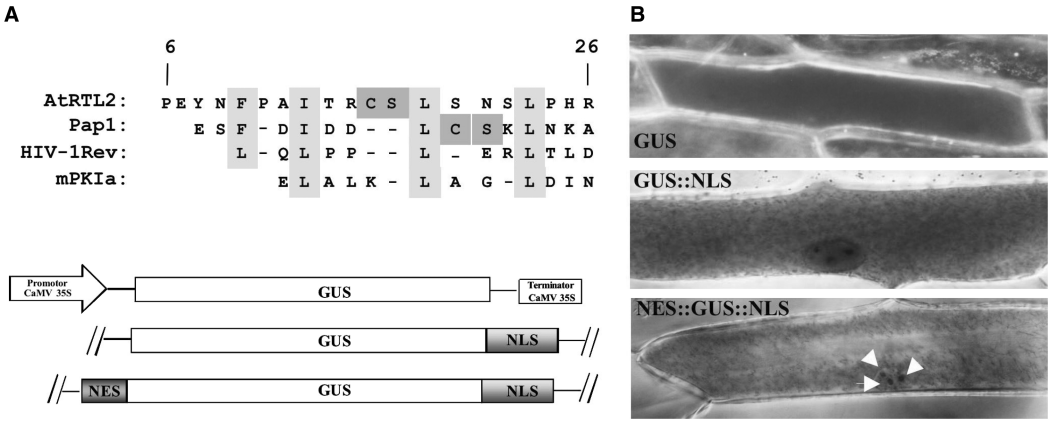

Figure 6. AtRTL2 contains a nuclear export signal (NES). (**A**) Alignment of putative NES sequences from AtRTL2 with NES from Pap1; HIV-1Rev and mPKIα (top). Schematic representation of GUS, GUS::NLS and NES::GUS::NLS constructs (bottom). (**B**) Onion epidermal cell transformed with GUS alone (upper panel), GUS fused to the nuclear localization signal (NLS) of RPL13 (middle panel) and the GUS::NLS construct fused to the N-terminal sequence of AtRLT2 containing a putative NES (bottom panel). White arrows show three nuclear bodies containing unexported GUS activity.

soluble protein extracts prepared from *Arabidopsis* flower buds were fractionated through a size fractionation Sephacryl S300 column equilibrated either with 0.1 M KCl or 0.5 M KCl buffer (Figure 7A). Western blot analyses of eluted fractions revealed that the peak of AtRTL2 protein eluted at ~110 kDa in both conditions (lanes 69–75). The estimated size corresponds approximately to at least twice the predicted molecular weight of AtRTL2 (~45 kDa), suggesting that the AtRTL2 protein exists as a dimer. We did not detect AtRTL2 protein in higher molecular weight fractions (lanes 57–67). Protein fractions of molecular weight lower than 67 kDa eluted as a large and diluted bulk of proteins, making the detection of AtRTL2 difficult. Consequently we could not determine to what extent AtRTL2 may exist as a monomer, if at all.

The AtRTL2 protein sequence contains five cysteines (C14, C86, C240, C322 and C348) among which two (C240 and C322) are conserved in the rice ortholog OsRTL2 (Figure 2B). Consequently, we tested the ability of AtRTL2 to dimerize through intermolecular disulfide bonds. For this purpose, refolded recombinant protein His-AtRTL2 (see Materials and Methods section) was first subjected to different reducing treatments before migration on a denaturing polyacrylamide gel. As shown in Figure 7B, His-AtRTL2 protein treated with 120 mM DTT remained mostly as monomers (lane 1), whereas at a lower DTT concentration His-AtRTL2 behaved as a dimer (12 mM DTT, lane 2) or as larger species (1.2 mM DTT, lane 3). Much lower amounts of DTT induced formation of even larger forms that probably do not enter the gel and are consequently not detected (lane 4).

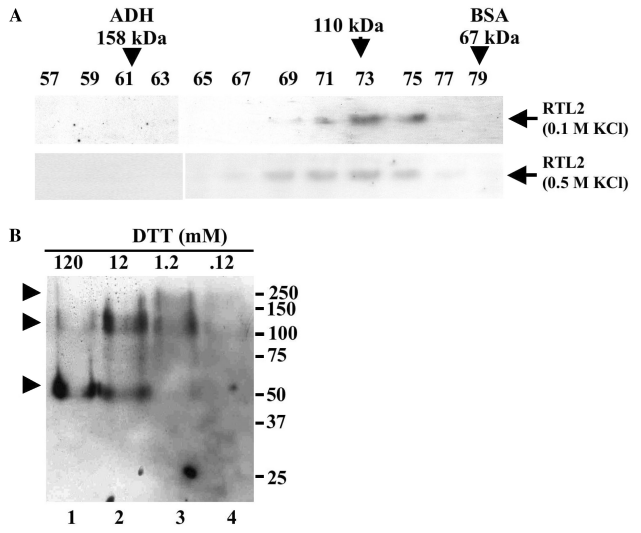

Figure 7. Redox regulation of AtRTL2 protein dimerization. (**A**) Gel filtration chromatographic analysis of AtRTL2 under 0.1 M KCl (top) or 0.5 M KCl (bottom) buffer conditions. Numbered lines correspond to the protein fractions (from 57 to 79). The peak position of alcohol dehydrogenase (ADH, 158 kDa) and bovine serum albumin (BSA, 67 kDa) markers are indicated by arrowheads. The arrow at the 110 kDa position indicates the estimated size of the RTL2 protein peak. (**B**) Recombinant His-AtRTL2 protein in sample buffer containing 120, 12, 1.2 and 0.12 mM DTT (lanes 1–4) was analyzed by SDS–PAGE and western blot with α-AtRTL2 antibodies. Arrows indicate positions of monomers, dimers and higher order structures according to standard molecular weight markers.

The recombinant His-AtRTL2 protein showed similar behavior after incubation with different amounts of another reducing agent, β-mercaptoethanol (data not shown). Finally, fractionation of His-AtRTL2 recombinant protein throughout sucrose gradients demonstrates that His-AtRTL2 homodimer formation is indeed dependent on DTT (Figure S3A). Moreover, in protein extracts from *Arabidopsis* the amount of AtRTL2 monomer protein was also dependent on DTT concentration (Figure S3B).

In conclusion, these data suggest that AtRTL2 forms homodimers through the formation of disulfide bonds.

Disruption of AtRTL2 by a T-DNA insertion inhibits cleavage of the 3′ETS from rRNA precursor

To investigate the functional role of AtRTL2 *in planta*, an *AtRtl2* homozygous line was isolated. In this mutant line (Gabi-Kat line 568D10), expression of the *AtRTL2* gene was disrupted by a T-DNA insertion as shown in Figure 8A. RT-PCR analysis using primers *5′rtl2* and *3′rtl2* did not detect *AtRTL2* transcripts in *AtRtl2* mutant plants (Figure 8B, RT-PCR panel, lane 2) compared with WT plants (lane 1). In addition, to verify the absence of the AtRTL2 protein, we performed western blot analysis using antibodies against His-AtRTL2 (α-AtRTL2 panel). Indeed, α-AtRTL2 detected a ~45 kDa polypeptide in WT nuclear protein extracts (lane 1) which is absent in the *AtRtl2* nuclear protein extract (lane 2).

To test whether or not the processing of polycistronic snoRNA and 3′ETS pre-rRNA precursors was affected in *AtRtl2* plants, total RNA was extracted from WT and *AtRtl2* plants and the accumulation of snoRNA monocistronic (U3), dicistronic (tsnoRNA), polycistronic (cluster 15) and 3′ETS pre-rRNA was measured by semi-quantitative RT-PCR. As shown in Figure 8B, we observed significant accumulation of a band corresponding to the unprocessed 3′ETS from the rRNA precursor in *AtRtl2* plants (panel At3′ETS, lane 4) compared with WT plants (lane 3). In contrast, we detected no major effect on the level of polycistronic snoRNA (panel cluster 15), nor on that of dicistronic (panel tsnoRNA R43.1) or monocistronic snoRNAs (panel snoRNA U3). We also observed that AtRTL2 does not cleave the pre-RNA precursor at the P site in the 5′ETS (44) (Figure S2). This is in agreement with results in yeast that demonstrate that Rnt1 is required for cleavage of pre-rRNA in the 3′ETS but not the 5′ETS (2). In conclusion these results (Figures 8B and S4) demonstrate that AtRTL2 cleaves the 3′ETS from the rRNA precursor in *planta*.

DISCUSSION

Here we report the functional study of AtRTL2, an RNaseIII-like protein that belongs to a small family of three genes in *A. thaliana* (*AtRTL1*, *AtRTL2* and *AtRTL3*). Based on the protein structure, AtRTL2 can be considered as a class II and AtRTL3 as a class III RNaseIII-like protein. As the AtRTL1 protein sequence does not contain a conserved dsRNA RBD, it does not fit any of these classes. The RTL1, -2 and -3 protein sequences are found not only in dicotyledons, but also in monocotyledonous plants, suggesting evolutionary and functional conservation (Figure 1). We were not able to identify genes encoding these proteins in other plant species because most available plant sequences are truncated cDNA or unfinished DNA sequence programs. However, the fact that the proteins are found in both Arabidopsis and rice strongly suggests their presence in all plant lineages.

The *AtRTL2* gene is constitutively expressed in all organs and plant tissues tested. *AtRTL1* is expressed mainly in roots and we have never detected *RTL3* transcripts in our growth conditions, or in the *Arabidopsis* MPSS databanks (www.mpss.udel.edu/at/). Thus, in standard growth conditions only *AtRTL2*, and to some extent *AtRTL1*, seem to be functional genes in *A. thaliana* (Figure 3). However, only *AtRTL2* seems to play a more general role.

AtRTL2 expression is controlled at the transcriptional and/or post-transcriptional level. Indeed, although *AtRTL2* transcripts are detected in all tissues and plant organs tested, no protein is detected in dry seeds (Figure 4). In fact, the AtRTL2 protein level decreased during seed formation and became detectable after seed imbibition. Accumulation of different RNAs, including rRNA precursors and mRNA in seeds was reported several years ago (57,58). These reports show that, whereas some RNAs are degraded during seed formation, other are stored and used as soon as germination starts. Thus, *AtRTL2* transcript accumulation in dry seeds could constitute a mechanism to

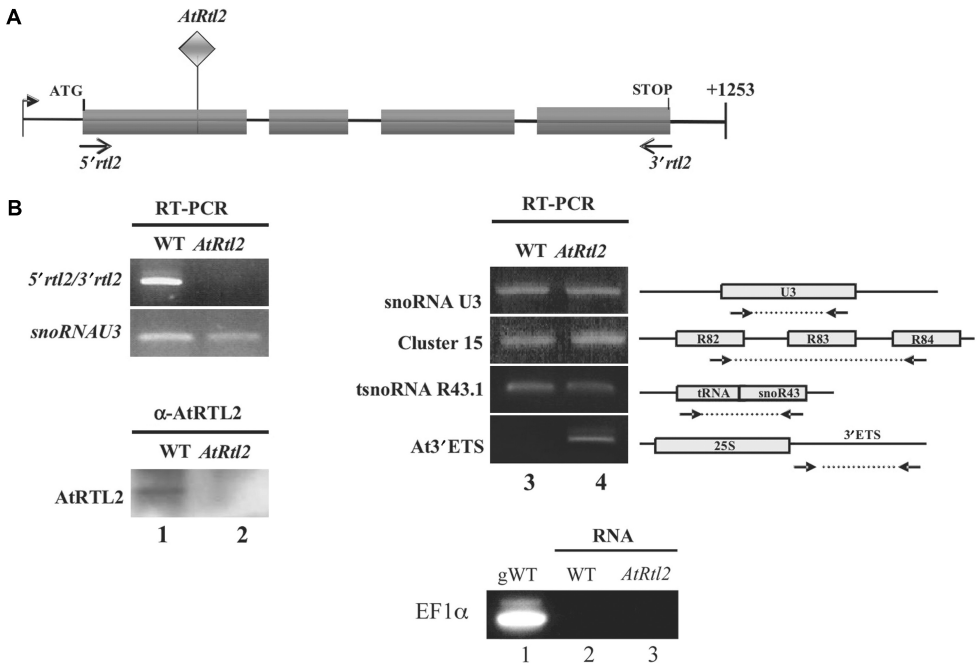

Figure 8. Analysis of *A. thaliana* plants with an *AtRTL2* gene disrupted by T-DNA insertion. (**A**) Diagram of *AtRTL2* gene transcript including 5′UTR and 3′UTR. Gray boxes correspond to exons separated by three introns. The T-DNA insertion in *AtRtl2* plants is indicated by a gray diamond. Positions of primers *5′rtl2* and *3′rtl2* used to detect *AtRTL2* transcripts are indicated by black arrows. (**B**) Left panel: RT-PCR reaction using total RNA isolated from 15-day WT and *AtRtl2* seedlings (lanes 1 and 2) to detect *AtRTL2* transcripts. Detection of the U3snoRNA transcript was performed as an RT-PCR control to evaluate the amount of RNA used in each reaction (bottom). Lower panel: nuclear protein fractions from WT and *Atrtl2* (lanes 1 and 2) were fractionated by SDS–PAGE and hybridized with α-AtRTL2 antibody. Right panel: RT-PCR reaction using total RNA isolated from 15-day seedlings (WT and *AtRtl2* plants lanes 3–4) to detect monocistronic (snoRNA U3) and polycistronic snoRNA precursors (cluster 15), tsnoRNA R43.1 and the 3′ETS from pre-rRNA (At3′ETS). Schematic representation of genomic organization of snoRNA U3, cluster 15 snoRNA, tsnoRNA R43.1 and the 3′ETS to show positions of primers used for amplification in the RT-PCR reaction. Panel EF1α shows a PCR reaction using genomic DNA extracted from WT plants (lane 1) or total RNA extracted from WT (lane 2) or *AtRtl2* (lane 3) plants.

ensure rapid synthesis of RNaseIII protein for efficient growth and plant development. Further experiments are required to confirm these hypotheses.

AtRTL2 localizes both in the nucleus and cytoplasm of *A. thaliana* cells (Figure 5). We would expect that protein modification allows AtRTL2 to move in and out of the nucleus to carry out multiple cellular functions in response to different physiological and/or cell conditions. In agreement with this, it has been demonstrated that the nuclear localization of human RNaseIII and yeast Rnt1 is cell-cycle dependent (3,18). The nuclear-cytoplasmic localization of AtRTL2 seems to be controlled by a novel nuclear export signal (NES) located in the N-terminal part of the protein (Figure 6). Strikingly, although NES are defined rather as short hydrophobic leucine and isoleucine-rich sequences, three amino acid residues, CSL and LCS, are conserved in both AtRTL2 and Pap1 NES sequences respectively (Figure 6A). This observation is important because the two cysteines in the Pap1 NES have been implicated in nuclear-cytoplasmic relocalization of Pap1 in response to oxidative stress (56).

In silico analysis and biochemical studies indicate that AtRTL2 forms homodimers and cleaves intergenic RNA regions (Figures 2, 3 and Supplementary Figure S3), as do bacterial RNaseIII (15) and yeast Rnt1 (25,59) proteins. However, the mechanisms involved in target recognition or dimer formation appear to be different. Indeed, we could not obtain predicted folding of the dsRBD of AtRTL2 based in crystal structures from bacterial RNaseIII (22,49) or yeast Rnt1 (50) proteins. This is an important observation because the dsRBD of RNaseIII and Rnt1 proteins positions the ribonuclease domain on the cleavage site in a ruler-like mechanism (28). Moreover, stems capped with the conserved AGNN or AAGU tetra loops sequence identified in yeast, were not identified in the 3′ETS sequence of *Arabidopsis* pre-rRNA. Only an inverted tetra loop sequence was found in the polycistronic snoRNA cluster 15 (Figure S3).

On the other hand, Rnt1 contains an extended N-terminal domain required for dimerization that is absent in the AtRTL2 and bacterial RNaseIII proteins (Figures 1 and 2). Nevertheless, our results clearly show that AtRTL2 is capable of dimerization, most probably forming homodimers, indicating that another mechanism for such dimerization was required. First, we tested whether hydrophobic interactions between RNaseIII domains of two AtRTL2 proteins could be responsible for dimerization, since similar mechanisms have been proposed for bacterial RNaseIII (15). Hydrophobic interactions have also been recently described as a requirement for homodimerization of some members of the DEDD exonucleases such as *E. coli* RNase T exoribonuclease (60) and bacterial oligoribonuclease (61). In the case of AtTRL2 however, we found that the

AtRTL2 dimer is resistant to high salt concentration, suggesting that hydrophobic interactions might not be the predominant mechanism for dimerization. Next, without completely excluding the possibility that hydrophobic cores may play a role at the dimer interface, we considered the possibility that other signals such as the presence of cysteine residues forming disulfide bridges could orchestrate AtRTL2 dimerization. Stabilization of protein complexes through establishment of disulfide bridges has been demonstrated in numerous examples, including some RNase proteins such as the yeast and human protein kinase/endoribonucleases IRE1α (62). Interestingly, we found that the AtRTL2 protein contains 5 cysteines, among which Cys240 and Cys322, located in the C-terminal region, are conserved in the orthologous rice RTL2 protein (Figure 2B). In contrast to the conserved Cys168 in RNase T proteins that is required for dimerization exclusively through its hydrophobic properties (60,63), we have demonstrated here that homodimerization of AtRTL2 is controlled by disulfide bond formation (Figures 7 and S3). However, whether or not Cys240 and Cys322 are dimerization signals controlling the dynamics and activity of AtRTL2 now remains to be elucidated. Different hypotheses are now open. AtRTL2 could either form intra molecular bonds giving rise to conformational changes required prior to the dimerization event, possibly followed by other requirements such as hydrophobic interactions, hydrogen-bond networks or intermolecular disulfide(s) bridging monomers to stabilize AtRTL2 as a functional dimer. Analysis of the three-dimensional structure of AtRTL2 as well as the use of AtRTL2 variants carrying mutated cysteines should provide more information regarding the role of these cysteine residues.

We show that disruption of the *AtRTL2* gene by a T-DNA insertion (*AtRtl2* plants) inhibits cleavage of the 3′ETS of pre-rRNA *in planta* (Figures 8 and S4). This is in agreement with the nuclear localization of AtRTL2 and the reported role of RNaseIII and RNaseIII-like proteins in ribosome biogenesis in eukaryotic cells (64,65). The *AtRtl*2 plants do not display any growth or morphological phenotype. This is unlike the slow growth phenotype observed in *S. cerevisiae* in which the Rnt1p gene has been deleted (4). In this context, we can speculate that cleavage of the 3′ETS of pre-RNA is not strictly required for cell function and/or *Arabidopsis* plant development. It is also possible that in the *AtRtl2* mutant plants, functions of AtRTL2 are carried out by other proteins containing RNaseIII domains. However, if this is the case, the cleavage activity is probably much slower than that of AtRTL2 due to the strong accumulation of uncut 3′ETS in the plant mutant. The *Arabidopsis* genome encodes four dicer-like proteins that could possibly replace some of the AtRTL2 activities (19,20).

Interestingly, in the *AtRtl2* plants, the level of polycistronic snoRNA precursors is not affected as expected (Figure 8). The 3′ETS cleavage of pre-rRNA is a co-transcriptional processing step that takes place in the nucleolus (31), whereas processing of snoRNA is carried out not only in the nucleoplasm (66) but also in the nucleolus and Cajal bodies (67). In this context, it is possible that disruption of AtRTL2 does not affect polycistronic snoRNA because other factors take over the role of AtRTL2, such us a Dicer-like protein (19,20) or the AtRTL1 protein as mentioned above. However, we cannot discard the possibility that polycistronic snoRNA are processed by a mechanism that does not involve RNaseIII-like activities. Indeed, although hairpin-loop structures can be predicted between the snoRNA coding sequences R82, R83 and R84 from cluster 15, only the hairpin-loop structure located between snoRNA R82 and R83 is stem-capped with the conserved AGNN sequence identified in yeast (Figure S2).

In conclusion, AtRTL2 is a double-stranded RNaseIII endonuclease-like protein but the molecular bases controlling the activities of AtRTL2 are probably different from those of bacterial RNaseIII and yeast Rnt1 proteins. Indeed, redox regulation might play a key role both in the cellular localization and the protein dynamics of AtRTL2. On the other hand, it is most likely that AtRTL2 is involved in processing of other RNAs both in the nucleus and the cytoplasm. The identification of targets and mechanisms controlling the activity and dynamics of AtRTL2 is the next challenge to contribute to a better understanding of how RNAs and RNaseIII-like proteins control gene expression in higher eukaryotes.

SUPPLEMENTARY DATA

Supplementary Data are available at NAR online.

ACKNOWLEDGEMENTS

The authors wish to thank our fellow lab members for stimulating discussions. We thank Dr Yves Meyer for critical reading of the manuscript. We would also like to thank R. Cooke for comments and correction of the English and J. R. Pages and M. Bangratz-Reyser for computer artwork and technical assistance, respectively. This work was supported by the Centre National de la Recherche Scientifique (CNRS). F.P. and N.B. were supported by a fellowship from Ministère de l'Enseignement et de la Recherche. Funding to pay the Open Access publication charges for this article was provided by CNRS.

Conflict of interest statement. None declared.

REFERENCES

1. Ivakine,E., Spasov,K., Frendewey,D. and Nazar,R.N. (2003) Functional significance of intermediate cleavages in the 3′ETS of the pre-rRNA from Schizosaccharomyces pombe. *Nucleic Acids Res.*, **31**, 7110–7116.
2. Kufel,J., Dichtl,B. and Tollervey,D. (1999) Yeast Rnt1p is required for cleavage of the pre-ribosomal RNA in the 3′ ETS but not the 5′ ETS. *RNA*, **5**, 909–917.
3. Wu,H., Xu,H., Miraglia,L.J. and Crooke,S.T. (2000) Human RNase III is a 160-kDa protein involved in preribosomal RNA processing. *J. Biol. Chem.*, **275**, 36957–36965.
4. Chanfreau,G., Legrain,P. and Jacquier,A. (1998) Yeast RNase III as a key processing enzyme in small nucleolar RNAs metabolism. *J. Mol. Biol.*, **284**, 975–988.

5. Chanfreau,G., Rotondo,G., Legrain,P. and Jacquier,A. (1998) Processing of a dicistronic small nucleolar RNA precursor by the RNA endonuclease Rnt1. *EMBO J.*, **17**, 3726–3737.
6. Ghazal,G., Ge,D., Gervais-Bird,J., Gagnon,J. and Abou Elela,S. (2005) Genome-wide prediction and analysis of yeast RNase III-dependent snoRNA processing signals. *Mol. Cell Biol.*, **25**, 2981–2994.
7. Giorgi,C., Fatica,A., Nagel,R. and Bozzoni,I. (2001) Release of U18 snoRNA from its host intron requires interaction of Nop1p with the Rnt1p endonuclease. *EMBO J.*, **20**, 6856–6865.
8. Qu,L.H., Henras,A., Lu,Y.J., Zhou,H., Zhou,W.X., Zhu,Y.Q., Zhao,J., Henry,Y., Caizergues-Ferrer,M. *et al.* (1999) Seven novel methylation guide small nucleolar RNAs are processed from a common polycistronic transcript by Rat1p and RNase III in yeast. *Mol. Cell Biol.*, **19**, 1144–1158.
9. Abou Elela,S. and Ares,M. Jr (1998) Depletion of yeast RNase III blocks correct U2 3′ end formation and results in polyadenylated but functional U2 snRNA. *EMBO J.*, **17**, 3738–3746.
10. Chanfreau,G., Elela,S.A., Ares,M. Jr and Guthrie,C. (1997) Alternative 3′-end processing of U5 snRNA by RNase III. *Genes Dev.*, **11**, 2741–2751.
11. Danin-Kreiselman,M., Lee,C.Y. and Chanfreau,G. (2003) RNAse III-mediated degradation of unspliced pre-mRNAs and lariat introns. *Mol. Cell*, **11**, 1279–1289.
12. Ge,D., Lamontagne,B. and Elela,S.A. (2005) RNase III-mediated silencing of a glucose-dependent repressor in yeast. *Curr. Biol.*, **15**, 140–145.
13. MacRae,I.J. and Doudna,J.A. (2007) Ribonuclease revisited: structural insights into ribonuclease III family enzymes. *Curr. Opin. Struct. Biol.*, **17**, 138–145.
14. Filippov,V., Solovyev,V., Filippova,M. and Gill,S.S. (2000) A novel type of RNase III family proteins in eukaryotes. *Gene*, **245**, 213–221.
15. Nicholson,A.W. (1999) Function, mechanism and regulation of bacterial ribonucleases. *FEMS Microbiol. Rev.*, **23**, 371–390.
16. Allmang,C. and Tollervey,D. (1998) The role of the 3′ external transcribed spacer in yeast pre-rRNA processing. *J. Mol. Biol.*, **278**, 67–78.
17. Rotondo,G. and Frendewey,D. (1996) Purification and characterization of the Pac1 ribonuclease of Schizosaccharomyces pombe. *Nucleic Acids Res.*, **24**, 2377–2386.
18. Catala,M., Lamontagne,B., Larose,S., Ghazal,G. and Elela,S.A. (2004) Cell cycle-dependent nuclear localization of yeast RNase III is required for efficient cell division. *Mol. Biol. Cell.*, **15**, 3015–3030.
19. Hiraguri,A., Itoh,R., Kondo,N., Nomura,Y., Aizawa,D., Murai,Y., Koiwa,H., Seki,M., Shinozaki,K. *et al.* (2005) Specific interactions between Dicer-like proteins and HYL1/DRB-family dsRNA-binding proteins in Arabidopsis thaliana. *Plant Mol. Biol.*, **57**, 173–188.
20. Pontes,O., Li,C.F., Nunes,P.C., Haag,J., Ream,T., Vitins,A., Jacobsen,S.E. and Pikaard,C.S. (2006) The Arabidopsis chromatin-modifying nuclear siRNA pathway involves a nucleolar RNA processing center. *Cell*, **126**, 79–92.
21. Provost,P., Dishart,D., Doucet,J., Frendewey,D., Samuelsson,B. and Radmark,O. (2002) Ribonuclease activity and RNA binding of recombinant human Dicer. *EMBO J.*, **21**, 5864–5874.
22. Blaszczyk,J., Gan,J., Tropea,J.E., Court,D.L., Waugh,D.S. and Ji,X. (2004) Noncatalytic assembly of ribonuclease III with double-stranded RNA. *Structure*, **12**, 457–466.
23. Blaszczyk,J., Tropea,J.E., Bubunenko,M., Routzahn,K.M., Waugh,D.S., Court,D.L. and Ji,X. (2001) Crystallographic and modeling studies of RNase III suggest a mechanism for double-stranded RNA cleavage. *Structure*, **9**, 1225–1236.
24. March,P.E. and Gonzalez,M.A. (1990) Characterization of the biochemical properties of recombinant ribonuclease III. *Nucleic Acids Res.*, **18**, 3293–3298.
25. Lamontagne,B., Tremblay,A. and Abou Elela,S. (2000) The N-terminal domain that distinguishes yeast from bacterial RNase III contains a dimerization signal required for efficient double-stranded RNA cleavage. *Mol. Cell. Biol.*, **20**, 1104–1115.
26. Nagel,R. and Ares,M. Jr (2000) Substrate recognition by a eukaryotic RNase III: the double-stranded RNA-binding domain of Rnt1p selectively binds RNA containing a 5′-AGNN-3′ tetraloop. *RNA*, **6**, 1142–1156.
27. Allas,U., Liiv,A. and Remme,J. (2003) Functional interaction between RNase III and the Escherichia coli ribosome. *BMC Mol. Biol.*, **4**, 8.
28. Chanfreau,G., Buckle,M. and Jacquier,A. (2000) Recognition of a conserved class of RNA tetraloops by Saccharomyces cerevisiae RNase III. *Proc. Natl Acad. Sci. USA*, **97**, 3142–3147.
29. Gaudin,C., Ghazal,G., Yoshizawa,S., Elela,S.A. and Fourmy,D. (2006) Structure of an AAGU tetraloop and its contribution to substrate selection by yeast RNase III. *J. Mol. Biol.*, **363**, 322–331.
30. Lamontagne,B. and Abou Elela,S. (2007) Short RNA guides cleavage by eukaryotic RNase III. *PLoS ONE*, **2**, e472.
31. Henras,A.K., Bertrand,E. and Chanfreau,G. (2004) A cotranscriptional model for 3′-end processing of the Saccharomyces cerevisiae pre-ribosomal RNA precursor. *RNA*, **10**, 1572–1585.
32. Margis,R., Fusaro,A.F., Smith,N.A., Curtin,S.J., Watson,J.M., Finnegan,E.J. and Waterhouse,P.M. (2006) The evolution and diversification of Dicers in plants. *FEBS Lett.*, **580**, 2442–2450.
33. Schauer,S.E., Jacobsen,S.E., Meinke,D.W. and Ray,A. (2002) DICER-LIKE1: blind men and elephants in Arabidopsis development. *Trends Plant Sci.*, **7**, 487–491.
34. Bouche,N., Lauressergues,D., Gasciolli,V. and Vaucheret,H. (2006) An antagonistic function for Arabidopsis DCL2 in development and a new function for DCL4 in generating viral siRNAs. *EMBO J.*, **25**, 3347–3356.
35. Henderson,I.R., Zhang,X., Lu,C., Johnson,L., Meyers,B.C., Green,P.J. and Jacobsen,S.E. (2006) Dissecting Arabidopsis thaliana DICER function in small RNA processing, gene silencing and DNA methylation patterning. *Nat. Genet.*, **38**, 721–725.
36. Papp,I., Mette,M.F., Aufsatz,W., Daxinger,L., Schauer,S.E., Ray,A., van der Winden,J., Matzke,M. and Matzke,A.J. (2003) Evidence for nuclear processing of plant micro RNA and short interfering RNA precursors. *Plant Physiol.*, **132**, 1382–1390.
37. Park,W., Li,J., Song,R., Messing,J. and Chen,X. (2002) CARPEL FACTORY, a Dicer homolog, and HEN1, a novel protein, act in microRNA metabolism in Arabidopsis thaliana. *Curr. Biol.*, **12**, 1484–1495.
38. Schmitz,R.J., Hong,L., Fitzpatrick,K.E. and Amasino,R.M. (2007) DICER-LIKE 1 and DICER-LIKE 3 redundantly act to promote flowering via repression of FLOWERING LOCUS C in Arabidopsis thaliana. *Genetics*, **176**, 1359–1362.
39. Xie,Z., Allen,E., Wilken,A. and Carrington,J.C. (2005) DICER-LIKE 4 functions in trans-acting small interfering RNA biogenesis and vegetative phase change in Arabidopsis thaliana. *Proc. Natl Acad. Sci. USA*, **102**, 12984–12989.
40. Xie,Z., Kasschau,K.D. and Carrington,J.C. (2003) Negative feedback regulation of dicer-like1 in Arabidopsis by microRNA-guided mRNA degradation. *Curr. Biol.*, **13**, 784–789.
41. Kumar,S., Tamura,K. and Nei,M. (2004) MEGA3: Integrated software for molecular evolutionary genetics analysis and sequence alignment. *Brief Bioinform.*, **5**, 150–163.
42. Pontvianne,F., Matia,I., Douet,J., Tourmente,S., Medina,F.J., Echeverria,M. and Saez-Vasquez,J. (2007) Characterization of AtNUC-L1 reveals a central role of nucleolin in nucleolus organization and silencing of AtNUC-L2 gene in Arabidopsis. *Mol. Biol. Cell*, **18**, 369–379.
43. Laemmli,U.K. (1970) Cleavage of structural proteins during the assembly of the head of bacteriophage T4. *Nature*, **227**, 680–685.
44. Saez-Vasquez,J., Caparros-Ruiz,D., Barneche,F. and Echeverria,M. (2004) A plant snoRNP complex containing snoRNAs, fibrillarin, and nucleolin-like proteins is competent for both rRNA gene binding and pre-rRNA processing in vitro. *Mol. Cell Biol.*, **24**, 7284–7297.
45. Jacquot,J.P., Rivera-Madrid,R., Marinho,P., Kollarova,M., Le Marechal,P., Miginiac-Maslow,M. and Meyer,Y. (1994) Arabidopsis thaliana NAPHP thioredoxin reductase. cDNA characterization and expression of the recombinant protein in Escherichia coli. *J. Mol. Biol.*, **235**, 1357–1363.
46. Barneche,F., Steinmetz,F. and Echeverria,M. (2000) Fibrillarin genes encode both a conserved nucleolar protein and a novel small nucleolar RNA involved in ribosomal RNA methylation in Arabidopsis thaliana. *J. Biol. Chem.*, **275**, 27212–27220.
47. Saez-Vasquez,J., Gallois,P. and Delseny,M. (2000) Accumulation and nuclear targeting of BnC24, a Brassica napus ribosomal protein

corresponding to a mRNA accumulating in response to cold treatment. *Plant Science*, **156**, 35–46.
48. Elela,S.A., Igel,H. and Ares,M. Jr (1996) RNase III cleaves eukaryotic preribosomal RNA at a U3 snoRNP-dependent site. *Cell*, **85**, 115–124.
49. Gan,J., Tropea,J.E., Austin,B.P., Court,D.L., Waugh,D.S. and Ji,X. (2005) Intermediate states of ribonuclease III in complex with double-stranded RNA. *Structure*, **13**, 1435–1442.
50. Leulliot,N., Quevillon-Cheruel,S., Graille,M., van Tilbeurgh,H., Leeper,T.C., Godin,K.S., Edwards,T.E., Sigurdsson,S.T., Rozenkrants,N. *et al.* (2004) A new alpha-helical extension promotes RNA binding by the dsRBD of Rnt1p RNAse III. *EMBO J.*, **23**, 2468–2477.
51. Schmid,M., Davison,T.S., Henz,S.R., Pape,U.J., Demar,M., Vingron,M., Scholkopf,B., Weigel,D. and Lohmann,J.U. (2005) A gene expression map of Arabidopsis thaliana development. *Nat. Genet.*, **37**, 501–506.
52. Meurs,C., Basra,A.S., Karssen,C.M. and van Loon,L.C. (1992) Role of abscisic acid in the induction of desiccation tolerance in developing seeds of Arabidopsis thaliana. *Plant Physiol.*, **98**, 1484–1493.
53. Merkle,T. (2003) Nucleo-cytoplasmic partitioning of proteins in plants: implications for the regulation of environmental and developmental signalling. *Curr. Genet.*, **44**, 231–260.
54. Malim,M.H., McCarn,D.F., Tiley,L.S. and Cullen,B.R. (1991) Mutational definition of the human immunodeficiency virus type 1 Rev activation domain. *J. Virol.*, **65**, 4248–4254.
55. Wen,W., Meinkoth,J.L., Tsien,R.Y. and Taylor,S.S. (1995) Identification of a signal for rapid export of proteins from the nucleus. *Cell*, **82**, 463–473.
56. Kudo,N., Taoka,H., Toda,T., Yoshida,M. and Horinouchi,S. (1999) A novel nuclear export signal sensitive to oxidative stress in the fission yeast transcription factor Pap1. *J. Biol. Chem.*, **274**, 15151–15158.
57. Aspart,L., Cooke,R., Michaux-Ferriere,N. and Delseny,M. (1980) Ribosomal RNA synthesis in imbibing radish (Raphanus sativus) embryo axes. *Planta*, **148**, 17–23.
58. Aspart-Pascot,L., Delseny,M. and Guitton,Y. (1976) Occurrence of nucleoside polyphosphates in rapidly labelled RNA preparations from radish seedlings. *Planta*, **131**, 275–278.
59. Rotondo,G., Huang,J.Y. and Frendewey,D. (1997) Substrate structure requirements of the Pac1 ribonuclease from Schizosaccharmyces pombe. *RNA*, **3**, 1182–1193.
60. Zuo,Y., Zheng,H., Wang,Y., Chruszcz,M., Cymborowski,M., Skarina,T., Savchenko,A., Malhotra,A. and Minor,W. (2007) Crystal structure of RNase T, an exoribonuclease involved in tRNA maturation and end turnover. *Structure*, **15**, 417–428.
61. Wu,Y.Y., Chin,K.H., Chou,C.C., Lee,C.C., Shr,H.L., Gao,F.P., Lyu,P.C., Wang,A.H. and Chou,S.H. (2005) Cloning, purification, crystallization and preliminary X-ray crystallographic analysis of XC847, a 3′-5′ oligoribonuclease from Xanthomonas campestris. *Acta Crystallogr. Sect. F Struct. Biol. Cryst. Commun.*, **61**, 902–905.
62. Liu,C.Y., Wong,H.N., Schauerte,J.A. and Kaufman,R.J. (2002) The protein kinase/endoribonuclease IRE1alpha that signals the unfolded protein response has a luminal N-terminal ligand-independent dimerization domain. *J. Biol. Chem.*, **277**, 18346–18356.
63. Li,Z., Zhan,L. and Deutscher,M.P. (1996) Escherichia coli RNase T functions in vivo as a dimer dependent on cysteine 168. *J. Biol. Chem.*, **271**, 1133–1137.
64. Fromont-Racine,M., Senger,B., Saveanu,C. and Fasiolo,F. (2003) Ribosome assembly in eukaryotes. *Gene*, **313**, 17–42.
65. Venema,J. and Tollervey,D. (1999) Ribosome synthesis in Saccharomyces cerevisiae. *Annu. Rev. Genet.*, **33**, 261–311.
66. Bachellerie,J.P., Cavaille,J. and Huttenhofer,A. (2002) The expanding snoRNA world. *Biochimie*, **84**, 775–790.
67. Shaw,P.J., Beven,A.F., Leader,D.J. and Brown,J.W. (1998) Localization and processing from a polycistronic precursor of novel snoRNAs in maize. *J. Cell Sci.*, **111**, 2121–2128.